American Mineralogist, Volume 97, pages 1821–1827, 2012

Cation ordering over short-range and long-range scales in the $MgAl_2O_4$-$CuAl_2O_4$ series

Rosa Anna Fregola,[1,*] Ferdinando Bosi,[2] Henrik Skogby,[3] and Ulf Hålenius[3]

[1]Dipartimento di Scienze della Terra e Geoambientali, Università di Bari Aldo Moro, via E. Orabona 4, I-70125 Bari, Italy
[2]Dipartimento di Scienze della Terra, Sapienza Università di Roma, Piazzale Aldo Moro 5, I-00185 Roma, Italy
[3]Department of Mineralogy, Swedish Museum of Natural History, SE-10405 Stockholm, Sweden

Abstract

A multi-analytical approach using electron microprobe analysis, X-ray structural refinement, and optical absorption spectroscopy was applied to characterize short-range and long-range structures of synthetic spinel single crystals along the $MgAl_2O_4$-$CuAl_2O_4$ solid-solution series. Site populations, derived from the results of site-scattering refinement and stereochemical analysis, show that the tetrahedrally coordinated site (T) is mainly populated by Mg and Cu^{2+}, while the octahedrally coordinated site (M) is dominated by Al. Crystals also show a significant degree of inversion, i.e., occurrence of Al at T counterbalanced by occurrence of divalent cations at M, which increases slightly from 0.24 to 0.29 for the highest Cu^{2+} contents.

Short-range information derived from optical spectra suggests that the local $^{T}Cu^{2+}$-O distances remain constant at increasing Cu^{2+} content, whereas local $^{M}Cu^{2+}$-O distances are ca. 0.02 Å shorter in Cu-poor $MgAl_2O_4$ spinels as compared to $^{M}Cu^{2+}$-O distances in end-member $CuAl_2O_4$. The observed splitting of an absorption band, at ca. 7000 cm^{-1}, caused by electron transitions in $^{T}Cu^{2+}$ as well as the anomalous broadness of an absorption band, at ca. 13 500 cm^{-1}, caused by electron transitions in $^{M}Cu^{2+}$ indicates the occurrence of local Jahn-Teller distortions at T and M. Long-range information, however, shows no violation of $Fd\bar{3}m$ symmetry. From refinements of our single-crystal XRD data we could for the first time derive for a cubic spinel phase a $^{M}Cu^{2+}$-O distance of 2.080 Å and a $^{T}Cu^{2+}$-O of 1.960 Å. The very limited variations in the unit-cell parameter *a* from 8.079 to 8.087 Å are mainly related to the disordering of Al. Because of the very similar size of Cu^{2+} and Mg at the T and M sites, the spinel structure responds to the $Cu^{2+} \rightarrow$ Mg substitution by increasing cation disordering in such a manner that mean M-O distances remain constant and the mean T-O distances decrease slightly. This results in increasing length of shared octahedral edges and thereby increase of the octahedral cation-cation repulsion. In line with other studies, the importance of steric factors for controlling the cation distributions in the spinel structure is demonstrated to be valid also in the $MgAl_2O_4$-$CuAl_2O_4$ solid-solution series.

Keywords: Copper spinel, electron microprobe, optical absorption spectroscopy, X-ray diffraction, cation ordering, ionic potential

Introduction

Several substances crystallize in the spinel type structure, most of which are multiple oxides. These latter may be defined by the general formula AB_2O_4, where A and B are usually divalent and trivalent cations (respectively), although tetravalent cations do also occur often (e.g., $FeTi_2O_4$, Bosi et al. 2008; Lenaz and Princivalle 2011). The spinel structure can be described as a slightly distorted cubic close packed array of oxygen anions, in which the A and B cations are distributed in one-eighth of all tetrahedrally coordinated sites (T) and half of all octahedrally coordinated sites (M). The unit-cell parameters (*a*, *a*, *a*) and oxygen fractional coordinates (*u*, *u*, *u*) define the resulting tetrahedral (T-O) and octahedral (M-O) bond lengths. The distribution of A and B cations over T and M leads to two different long-range ordered site populations: (1) normal spinel, where the A cation occupies T and the B cations occupy M (e.g., $MgAl_2O_4$ and $MgCr_2O_4$; Fregola et al. 2011; Lenaz et al. 2004) and (2) inverse spinel, where half of the B cations occupy T and the remaining A and B cations occupy M (e.g., $FeFe_2O_4$ and $MgFe_2O_4$; Bosi et al. 2009; Lenaz et al. 2006). The spinel structure symmetry is typically cubic $Fd\bar{3}m$, but also tetragonal $I4_1/amd$ phases occur as a result of Jahn-Teller distortion imposed by cations with unpaired *d*-electronic levels, such as those with high spin configuration d^4 (Mn^{3+}) and d^9 (Cu^{2+}), occupying octahedral or tetrahedral environments. Examples of the Jahn-Teller active ions in octahedral environment are given by the tetragonally distorted inverse cuprospinel $CuFe_2O_4$ (Prince and Treuting 1956) and hausmannite $MnMn_2O_4$ (Bosi et al. 2002), whereas the Jahn-Teller active ions in tetrahedral environment is shown by the tetragonally distorted normal spinel $CuCr_2O_4$ (Dollase and O'Neill 1997).

Although several studies were directed to the Cu-rich spinels as well as to the substitution of Cu^{2+} by a divalent cation (e.g., O'Neill et al. 2005; Le Nestour et al. 2007a, and references therein), a systematic investigation of the structural variations all along the entire $(Mg_{1-x}Cu_x)Al_2O_4$ solid-solution series is miss-

* E-mail: rosaanna.fregola@uniba.it

0003-004X/12/1112–1821$05.00/DOI: http://dx.doi.org/10.2138/am.2012.4177

ing. In the present work, we investigated by a combined crystallographic and spectroscopic approach spinel single crystals belonging to the $(Mg_{1-x}Cu_x)Al_2O_4$ series, produced by flux growth and chemically characterized by electron microprobe analyses, to reveal structural details and improve our understanding of the factors that affect cation distribution in spinel.

Experimental methods

Crystal synthesis

Single-crystal spinel samples of eight compositions distributed over the $MgAl_2O_4$-$CuAl_2O_4$ join were synthesized by a flux growth method, using $Na_2B_4O_7$ as flux compound. The starting material consisted of analytical grade oxides, which were dried before mixing by grinding under acetone in an agate mortar. The weight ratios of the flux:spinel components were adjusted according to the starting compositions and varied from 0.5 to 1.5, with the lower values for the $CuAl_2O_4$ end-member experiments. Around 7 g of starting material was loaded in 15 mL Pt/Au (5%) crucibles, which were covered by lids and inserted in a muffle furnace under ambient atmospheric conditions. The synthesis experiments were started by increasing the temperature to 1200 °C, where the temperature was kept constant for 24 h to achieve complete dissolution of the spinel components and homogenization of the melt. Subsequently, the temperature was slowly decreased (4 °/h) down to 800 °C, from where faster cooling down to room temperature was attained by turning off the heating power. Successful runs consisted of spinel and green colored Cu^{2+}-rich borate crystals embedded in borate-rich glass. Toward the Cu-rich end of the solid-solution series from run CuAl70 and run CuAl90, respectively, crystals of tenorite (CuO) and the delafossite-related compound $CuAlO_2$ were also present. The run products were treated in warm diluted HCl for 24 h to dissolve the glass. In successful runs, clear octahedral spinel crystals with sizes up to 1 mm could be extracted. The color of the spinel crystals shifts progressively from pale yellow for Cu-poor samples to brown and dark brownish red for Cu-rich samples (Fig. 1).

Electron microprobe analysis

The chemical compositions of the studied solid-solution crystals were determined by means of electron microprobe techniques, using a Cameca SX50 instrument operating at an accelerating potential of 15 kV and a sample current of 15 nA, with an incident beam size of ca. 1 µm. No less than 5 spot analyses for each sample were performed to obtain the average chemical compositions and estimates of compositional homogeneity. Synthetic standards used were MgO (Mg), Al_2O_3 (Al), and metallic Cu. For raw data reduction, the PAP computer program was applied (Pouchou and Pichoir 1984). Spinel formulas were calculated on the basis of 4 oxygen atoms per formula unit (Table 1).

Optical absorption spectroscopy

Unpolarized optical absorption spectra were recorded at room temperature using a circular measuring spot of 40 µm in diameter on double-sided polished single crystals ranging in thickness from 17 to 179 µm as determined by means of a digital micrometer. For spectrum recordings a Zeiss MPM800 microscope spectrometer

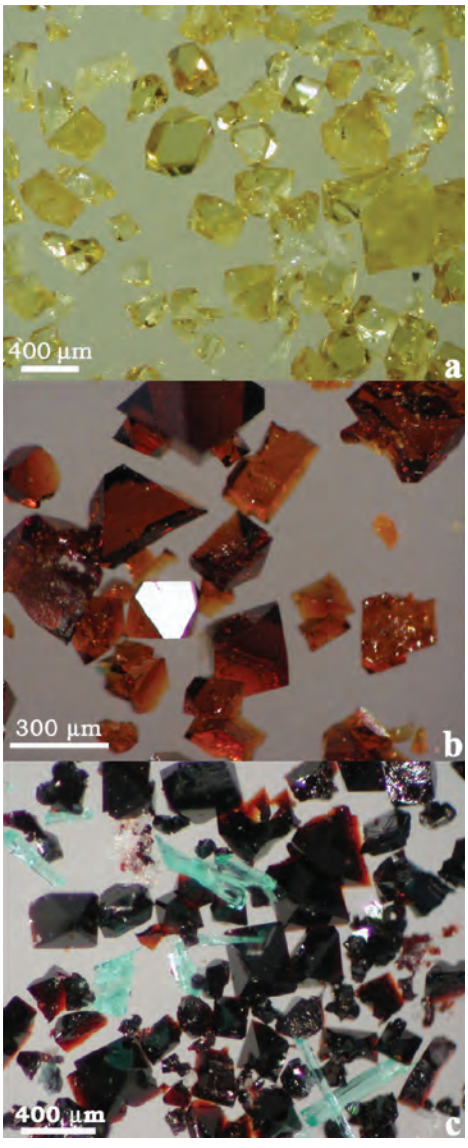

Figure 1. Microphotographs of solid-solution spinel single crystals (**a**) from run CuAl15a (0.06 apfu Cu), (**b**) from run CuAl50b (0.24 apfu Cu), and (**c**) from run CuAl90d (0.70 apfu Cu).

Table 1. Electron-microprobe analyses of the studied $Mg_{1-x}Cu_xAl_2O_4$ single crystals

Sample	CuAl05b	CuAl15a2	CuAl30bw	CuAl50bw	CuAl70aw	CuAl70bm	CuAl90dw	CuAl90dm	CuAl95b	CuAl100h
MgO wt%	27.75	26.55	24.88	20.59	15.27	14.54	7.61	7.33	4.96	0.00
CuO	0.68	3.05	6.54	12.46	20.81	22.35	32.87	33.12	36.21	42.87
Al_2O_3	71.60	70.94	69.47	67.98	64.78	64.40	61.04	60.45	60.21	57.48
Total	100.03	100.54	100.89	101.03	100.86	101.29	101.52	100.90	101.38	100.35
St.dev. wt%										
MgO	0.20	0.30	0.33	0.31	0.26	0.18	0.21	0.31	0.32	0.00
CuO	0.09	0.27	0.33	0.13	0.34	0.42	0.23	0.50	0.53	0.41
Al_2O_3	0.43	0.61	0.48	0.28	0.34	0.37	0.36	0.38	0.41	0.38
Cations on the basis of four O atoms										
Mg	0.982	0.946	0.900	0.766	0.595	0.569	0.315	0.306	0.210	0.000
Cu	0.012	0.055	0.120	0.235	0.411	0.443	0.689	0.701	0.775	0.967
Al	2.004	1.999	1.987	1.999	1.996	1.992	1.997	1.996	2.010	2.022
S.err apfu										
Mg	0.006	0.009	0.010	0.009	0.009	0.006	0.008	0.012	0.013	0.000
Cu	0.002	0.005	0.006	0.003	0.006	0.007	0.005	0.009	0.010	0.010
Al	0.006	0.010	0.010	0.008	0.009	0.008	0.008	0.012	0.013	0.010

Note: St.dev. = standard deviations of several spot analyses; S.err = standard errors calculated by error-propagation theory.

equipped with Ultrafluar 10× objective and condenser lenses, Xenon arc 75W and Halogen 100 W light sources, blazed concave monochromators and photomultiplier and photoconductive PbS-cell detectors, was used. Spectra were collected during three cycles at a resolution of 1 and 5 nm in the UV/VIS (330–800 nm) and NIR (800–2000 nm) spectral regions, respectively. The accuracy of determined absorption band energies in the UV/VIS-NIR region is estimated on the basis of measured Ho_2O_3-doped and Pr_2O_3/Nd_2O_3-doped calibration standards (Hellma glass filters 666-F1 and 666-F7) to be better than 60 cm^{-1}. Recorded spectra were fitted using the Jandel PeakFit 4.12 software assuming Gaussian peak shapes.

Single-crystal structural refinement

X-ray diffraction measurements were performed at the Earth Sciences Department, Sapienza University of Rome, with a Bruker KAPPA APEX-II single-crystal diffractometer, equipped with a CCD area detector (6.2 × 6.2 cm^2 active detection area, 512 × 512 pixels) and a graphite crystal monochromator, using Mo$K\alpha$ radiation from a fine-focus sealed X-ray tube. The sample-to-detector distance was 4 cm. A total of 4728 exposures per sample (step = 0.2°, time/step = 10 s) covering the full reciprocal sphere were collected. The orientation of the crystal lattice was determined from 500 to 1000 strong reflections ($I > 100\ \sigma_I$) evenly distributed in the reciprocal space, and used for subsequent integration of all recorded intensities. Final unit-cell parameters were refined by using the Bruker AXS SAINT program from more than 2000 recorded reflections with $I > 10\ \sigma_I$ in the range $8° < 2\theta < 90°$. The intensity data were processed and corrected for Lorentz, polarization, and background effects with the APEX2 software program of Bruker AXS. The data were corrected for absorption using multi-scan method (SADABS). The absorption correction led to a significant improvement in R_{int}. No violation of $Fd\bar{3}m$ symmetry was noted. Sporadic appearance of forbidden space-group reflections was recognized as double reflections.

Structural refinements were carried out with the SHELXL program (Sheldrick 2008). Setting the origin at $\bar{3}m$, initial atomic positions for oxygen atoms were taken from the structure of spinel (Bosi et al. 2007). Variable parameters were overall scale factor, extinction coefficient, atomic coordinates, site-scattering values expressed as mean atomic number (m.a.n.), and atomic displacement factors. No chemical constraint was applied during the refinement. To obtain the best values of statistical indexes ($R1$ and $wR2$) the oxygen site was modeled with neutral vs. fully ionized oxygen scattering curves, while neutral curves were used for the cation sites. In detail, the T site was modeled considering the presence of Mg and Cu scattering factors (except for the Mg-free sample CuAl100h, where Al and Cu were considered), whereas the M site was modeled by Al and Cu scattering factors. Three full-matrix refinement cycles with isotropic displacement parameters for all atoms were followed by anisotropic cycles until convergence was attained; that is when the shifts for all refined parameters were less than their estimated standard deviation. No correlation over 0.7 between parameters was observed at the end of refinement. Table 2 summarizes structural parameters and refinement details. (CIFs available on deposit[1].)

Cation distribution

The intracrystalline cation distribution was obtained by an optimization program applying a minimization function in which both structural and chemical data (such as bond lengths and site-scattering in terms of equivalent electrons, i.e., mean atomic number) are taken into account. The minimization procedure has been presented and discussed previously (Carbonin et al. 1996; Lavina et al. 2002; Bosi et al. 2004). Octahedral and tetrahedral bond lengths (M-O and T-O, respectively) were calculated as the linear contribution of each cation multiplied by its specific bond length. The latter were: ^{T}Mg-O = 1.966 Å, ^{M}Mg-O = 2.082 Å, ^{T}Al-O = 1.774 Å, and ^{M}Al-O = 1.908 Å, as refined on the basis of analysis of more than 250 spinel structural data from literature (Lavina et al. 2002). As for the specific bond length of Cu^{2+} at the T and M sites, no data for the cubic spinel phase are directly available in literature, to our knowledge. Consequently, as a first attempt to optimize the cation distribution, we used bond lengths derived from the ionic radii of Shannon (1976): $^{T}Cu^{2+}$-O = 1.950 Å and $^{M}Cu^{2+}$-O = 2.110 Å. These distances, however, resulted in high values in the minimization function. Considerable improvements in the minimization were obtained by using the $^{T}Cu^{2+}$-O = 1.960 Å measured by Tarantino et al. (2010) for the normal tetragonal spinel $CuCr_2O_4$. As for the $^{M}Cu^{2+}$-O distance, we refined a value of 2.080 Å, which yielded best fits for all examined crystals (i.e., all residuals were within the analytical uncertainty), and the final cation distributions (Table 3). It should be noted that this refined distance for $^{M}Cu^{2+}$-O = 2.080 Å is in excellent agreement with the value of 2.083 Å proposed by Burns and Hawthorne (1996) for an undistorted Cu^{2+}-centered octahedron.

[1] Deposit item AM-12-085, CIFs. Deposit items are available two ways: For a paper copy contact the Business Office of the Mineralogical Society of America (see inside front cover of recent issue) for price information. For an electronic copy visit the MSA web site at http://www.minsocam.org, go to the *American Mineralogist* Contents, find the table of contents for the specific volume/issue wanted, and then click on the deposit link there.

TABLE 2. Selected X-ray diffraction data for analyzed spinels in the $(Mg_{1-x}Cu_x)Al_2O_4$ series

Crystal	CuAl05b	CuAl15a2	CuAl30bw	CuAl50bw	CuAl70aw	CuAl70bm	CuAl90dw	CuAl90dm	CuAl95b	CuAl100h
Crystal size (mm)	0.15×0.19×0.2	0.20×0.20×0.22	0.14×0.14×0.16	0.15×0.16×0.18	0.12×0.13×0.15	0.12×0.18×0.26	0.18×0.20×0.24	0.15×0.16×0.18	0.16×0.16×0.18	0.10×0.12×0.14
a (Å)	8.0853(4)	8.0858(5)	8.0857(4)	8.0867(5)	8.0852(5)	8.0846(4)	8.0857(5)	8.0831(5)	8.0841(5)	8.0793(4)
u	0.26200(5)	0.26208(6)	0.26203(4)	0.26204(5)	0.26198(5)	0.26200(7)	0.26191(7)	0.26193(8)	0.26183(8)	0.26167(10)
T-O (Å)	1.9185(7)	1.9198(9)	1.9191(6)	1.9194(7)	1.9183(7)	1.9184(9)	1.9173(10)	1.9170(11)	1.9159(11)	1.9125(14)
M-O (Å)	1.9292(4)	1.9287(5)	1.9291(3)	1.9293(4)	1.9293(4)	1.9290(5)	1.9300(5)	1.9292(6)	1.9301(6)	1.9301(7)
T-m.a.n.	12.27(8)	12.92(11)	13.70(5)	14.63(5)	16.41(6)	16.59(8)	19.31(12)	19.71(14)	20.73(13)	24.11(21)
M-m.a.n.	12.94(4)	13.23(6)	13.46(3)	13.83(3)	14.44(4)	14.41(4)	15.08(7)	15.13(7)	15.29(6)	15.70(7)
T-U^{11} (Å^2)	0.0045(2)	0.0043(2)	0.0056(1)	0.0059(1)	0.0067(1)	0.0069(2)	0.0079(1)	0.0082(2)	0.0081(1)	0.0094(2)
M-U^{11} (Å^2)	0.0046(1)	0.0045(2)	0.0048(1)	0.00477(9)	0.00523(9)	0.0055(1)	0.0060(1)	0.0061(2)	0.0061(2)	0.0069(2)
M-U^{12} (Å^2)	−0.00014(4)	−0.00011(4)	−0.00021(4)	−0.00019(5)	−0.00024(5)	−0.00023(6)	−0.00027(6)	−0.00026(7)	−0.00029(7)	−0.00031(8)
O-U^{11} (Å^2)	0.0078(1)	0.0078(2)	0.0085(1)	0.0087(1)	0.0096(1)	0.0102(2)	0.0114(2)	0.0114(2)	0.0118(2)	0.0131(3)
O-U^{12} (Å^2)	0.00022(8)	0.00010(9)	0.00018(9)	0.00016(9)	0.0001(1)	0.0001(1)	0.0000(2)	0.0001(2)	−0.0001(2)	0.0001(2)
Reciprocal range *hkl*										
	$-16 \le h \le 16$	$-14 \le h \le 15$	$-15 \le h \le 16$	$-15 \le h \le 16$	$-10 \le h \le 11$	$-14 \le h \le 12$	$-15 \le h \le 16$	$-15 \le h \le 16$	$-14 \le h \le 11$	$-15 \le h \le 13$
	$-13 \le k \le 15$	$-14 \le k \le 11$	$-14 \le k \le 15$	$-12 \le k \le 14$	$-16 \le k \le 15$	$-16 \le k \le 15$	$-10 \le k \le 11$	$-15 \le k \le 15$	$-14 \le k \le 12$	$-12 \le k \le 14$
	$-10 \le l \le 16$	$-15 \le l \le 13$	$-14 \le l \le 10$	$-12 \le l \le 14$	$-16 \le l \le 14$	$-16 \le l \le 12$	$-15 \le l \le 16$	$-11 \le l \le 10$	$-16 \le l \le 16$	$-13 \le l \le 16$
Set of read reflections	2410	2417	2406	2435	2421	2411	2377	2424	2435	2416
Unique reflections	133	131	132	132	133	133	132	132	133	132
EXTI	0.173(8)	0.30(2)	0.053(2)	0.0154(9)	0.0067(6)	0.117(5)	0.0107(7)	0.041(2)	0.0193(9)	0.035(2)
R_{int} (%)	2.31	4.03	1.99	2.38	1.63	4.29	1.51	2.03	1.81	2.23
$R1$ (%) all reflections	1.79	2.54	1.28	1.23	1.20	1.71	1.45	1.60	1.52	1.89
$wR2$ (%)	4.17	5.55	3.05	2.92	2.88	3.50	2.87	3.51	3.05	4.24
Goof	1.223	1.350	1.155	1.106	1.168	1.254	1.108	1.241	1.162	1.217
Diff. peaks (±*e*/Å^3)	−0.44; 0.43	−0.71; 0.68	−0.28; 0.24	−0.28; 0.24	−0.30; 0.37	−0.54; 0.22	−0.47; 0.50	−0.43; 0.41	−0.48; 0.51	−0.46; 0.52

Notes: *a* = unit-cell parameter; *u* = oxygen fractional coordinate; T-O and M-O = tetrahedral and octahedral bond lengths, respectively; T- and M-m.a.n.. = T- and M-mean atomic number; U^{11} = atomic displacement parameter; $U^{11} = U^{22} = U^{33}$ and $U^{12} = U^{13} = U^{23}$ (=0 for *T*-site due to symmetry reasons); EXTI = extinction parameter; *R* int. = merging residual value; *R*1 = discrepancy index, calculated from *F*-data; *wR*2 = weighted discrepancy index, calculated from F^2-data; GooF = goodness of fit; Diff. peaks = maximum and minimum residual electron density. Radiation, Mo$K\alpha$ = 0.71073 Å. Data collection temperature = 293 K. Total number of frames = 4886. Range for data collection $8° < 2\theta < 91°$. Origin fixed at $\bar{3}m$. Space group $Fd\bar{3}m$. $Z = 8$ formula units. Spinel structure has cations at Wyckoff positions 8*a* ≡ T (1/8, 1/8, 1/8) and 16*d* ≡ M (1/2, 1/2, 1/2), and oxygen anions at 32*e* (*u*, *u*, *u*).

TABLE 3. Structural formulas of the analyzed $(Mg_{1-x}Cu_x)Al_2O_4$ spinels

Crystal	Formula
CuAl05b	$^{T}(Cu_{0.01}Mg_{0.75}Al_{0.24})^{M}(Mg_{0.24}Al_{1.76})O_4$
CuAl15a2	$^{T}(Cu_{0.03}Mg_{0.73}Al_{0.24})^{M}(Cu_{0.03}Mg_{0.21}Al_{1.76})O_4$
CuAl30bw	$^{T}(Cu_{0.07}Mg_{0.68}Al_{0.25})^{M}(Cu_{0.05}Mg_{0.20}Al_{1.75})O_4$
CuAl50bw	$^{T}(Cu_{0.14}Mg_{0.62}Al_{0.24})^{M}(Cu_{0.10}Mg_{0.14}Al_{1.76})O_4$
CuAl70aw	$^{T}(Cu_{0.24}Mg_{0.52}Al_{0.24})^{M}(Cu_{0.17}Mg_{0.07}Al_{1.75})O_4$
CuAl70bm	$^{T}(Cu_{0.26}Mg_{0.50}Al_{0.24})^{M}(Cu_{0.18}Mg_{0.06}Al_{1.76})O_4$
CuAl90dw	$^{T}(Cu_{0.43}Mg_{0.31}Al_{0.26})^{M}(Cu_{0.26}Al_{1.74})O_4$
CuAl90dm	$^{T}(Cu_{0.44}Mg_{0.30}Al_{0.26})^{M}(Cu_{0.26}Al_{1.74})O_4$
CuAl95b	$^{T}(Cu_{0.51}Mg_{0.22}Al_{0.27})^{M}(Cu_{0.27}Al_{1.73})O_4$
CuAl100h	$^{T}(Cu_{0.71}Al_{0.29})^{M}(Cu_{0.29}Al_{1.71})O_4$

Note: T = tetrahedrally coordinated site; M = octahedrally coordinated site; structural formulas optimized by assuming Al = 2.00 apfu and (Mg + Cu) = 1.00 apfu.

RESULTS AND DISCUSSION

The synthetic $(Mg_{1-x}Cu_x)Al_2O_4$ spinel crystals are characterized by the $Cu^{2+} \rightarrow Mg$ substitution with x ranging from 0.01 to 1. The site distribution of Mg, Cu^{2+}, and Al shows that the M site is dominated by Al and the T site is mainly populated by Mg and Cu^{2+} with a cation inversion, expressed as the occurrence of divalent cations at M sites, slightly increasing from 0.24 to 0.29 for the highest Cu^{2+} contents (Table 3). Furthermore, a marked atomic ordering also occurs among the divalent cations with Cu^{2+} preferentially accommodating at the M sites. This ordering can be quantified using the order parameter q (Andreozzi and Lucchesi 2002; Palin and Harrison 2007) defined as

$$^{IV}Cu^{2+} = (y + q)(1 - i)$$

where y is the total amount of Cu^{2+} and i is the inversion parameter. Positive q-values indicate ordering to the T site, whereas negative values indicate ordering to the M site. The Cu-Mg distribution for the studied samples results in negative q-values, with a minimum below –0.10 for the intermediate compositions. This can be compared with q-values close to +0.10 observed by Andreozzi and Lucchesi (2002) for $^{IV}Fe^{2+}$ in a series of $(Mg_{1-x}Fe_x)Al_2O_4$ spinels, indicating ordering of Fe^{2+} to the T site. The marked preference of Cu^{2+} (vs. Mg) for the octahedral coordination observed here is in line with the Cu^{2+} crystal-field stabilization energy.

Short-range structure

The recorded optical absorption spectra of the present crystals show three absorption features at ca. 7000, 13 500, and 24 000 cm^{-1} (Fig. 2). In detail, the feature at ca. 7000 cm^{-1} is skewed and it shows a distinct shoulder indicating that it is composed of two closely spaced absorption bands (ν_1 and ν_2 in Table 4). Although no distinct band shoulder is observed, the somewhat anomalous broadness (ca. 2500 cm^{-1}) for a single ion spin-allowed *d-d* transition indicates that the absorption band at ca. 13 500 cm^{-1} (ν_3 in Table 4) may also be split. Resolved spectra reveal only small energy variations for observed bands within the entire solid-solution range (Table 4). Bandwidths of individual bands remain also comparable throughout the entire compositional range. However, relative band intensities vary distinctly. The areas of the absorption features at ca. 7000 and 13 500 cm^{-1} increase linearly with Cu-content, while we observe that the area of the very broad absorption band at ca. 24 000 cm^{-1} (ν_4 in Table 4) displays a quadratic dependence on the Cu-content (Fig. 3) up to 0.41 apfu Cu. Due to very intense UV absorption in samples with higher Cu-content and difficulties in preparing sufficiently thin (<10 µm) self-supporting single-crystal absorbers, we were not able to record the intensity of this band in samples with higher Cu-concentrations. Similarly, high absorption values for all band features from the UV to the NIR region in combination with sample preparation limitations precluded measurement of the absorption spectrum of the end-member $CuAl_2O_4$ (sample CuAl100h).

The spectra of the present solid-solution spinel single crystals show overall similarities with diffuse reflectance spectra obtained on spinel powder samples in the $Zn_{1-x}Cu_xAl_2O_4$ solid-solution

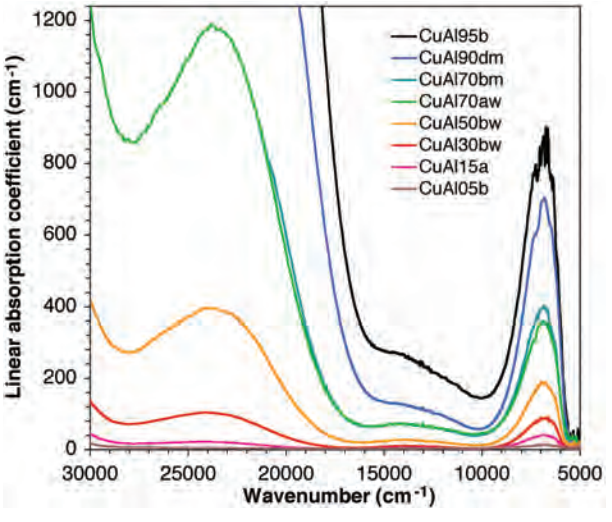

FIGURE 2. Optical absorption spectra of $Mg_{1-x}Cu_xAl_2O_4$ single crystals in the UV/VIS-NIR spectral range.

TABLE 4. Energies (ν), linear absorption coefficients (α), band widths ($w_{1/2}$), in cm^{-1}, and integrated absorption coefficients (A), in cm^{-2}, for recorded and fitted absorption bands

Sample	ν_1	α_1	$w_{1/2}$	A_1	ν_2	α_2	$w_{1/2}$	A_2	*Mean ν_1+ν_2	A_2+A_3	ν_3	α_3	$w_{1/2}$	A_3	ν_4	α_4	$w_{1/2}$	A_4
CuAl05b	6529	6	1004	6529	7450	7	1884	14480	7164	21009	13800	0.8	2350	2030	24000	2	6000	15924
CuAl15a	6595	25	984	26057	7463	26	1717	47651	7156	73708	13464	2	2800	7030	24310	20	6130	126910
CuAl30bw	6533	46	895	43568	7310	64	1718	117630	7100	161198	13577	6	2823	18039	23987	96	6065	615170
CuAl50bw	6568	100	987	104700	7359	127	1767	239700	7118	344400	13472	10	2414	25971	23512	349	5908	2183500
CuAl70aw	6588	206	1060	232530	7452	225	1798	428540	7148	661070	13377	15	2438	37549	23361	1020	6042	6534900
CuAl70bm	6599	242	1056	271940	7488	263	1767	495150	7173	767090	13129	16	3114	54590	no			
CuAl90dm	6547	396	999	420990	7411	467	1679	837510	7122	1258500	13084	18	2767	52045	no			
CuAl95b	6492	454	911	440800	7354	607	1670	1077900	7104	1518700	13146	24	2752	70220	no			

Notes: no = not observed due to too high absorption in the UV range. Estimated relative uncertainty for the band energies is 0.5%. Estimated relative uncertainties for α, $\omega_{1/2}$, and A values are 8%.
* Weighted mean energy of the split *d-d* transitions in $^{T}Cu^{2+}$.

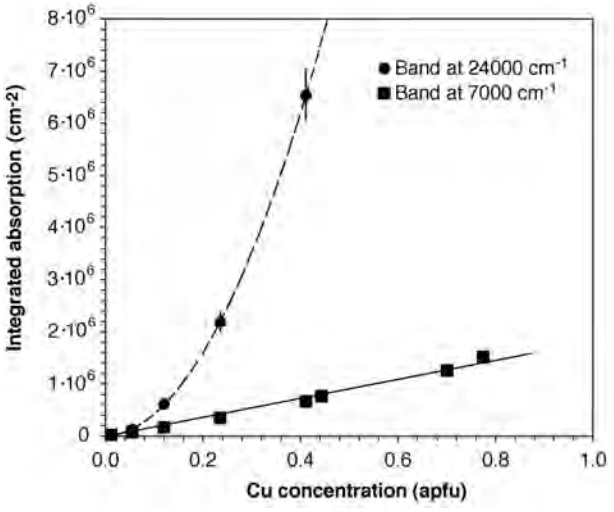

FIGURE 3. Integrated absorption of absorption bands at ca. 7000 and 24 000 cm^{-1} vs. Cu content for the $Mg_{1-x}Cu_xAl_2O_4$ spinel solid solution.

series (Le Nestour et al. 2007a, 2007b). In accordance with ligand field theory prediction and in parallel with their assignment, we assign the absorption band at ca. 13 500 cm^{-1} to a spin-allowed electronic *d-d* transition in octahedrally coordinated $^{M}Cu^{2+}$ and the absorption feature at ca. 7000 cm^{-1} to spin-allowed *d-d* transitions in tetrahedrally coordinated $^{T}Cu^{2+}$.

A broad absorption band at ca. 24 000 cm^{-1} in spectra of $Zn_{1-x}Cu_xAl_2O_4$ was assigned by Le Nestour et al. (2007a) to a O^{2-}-Cu^{2+} charge transfer transition, in which divalent copper cations at both T and M sites take part. The relatively low energy of the band in relation to the normal range for ligand-metal charge transfer bands involving transition metal cations in combination with our observed quadratic band intensity dependence on Cu-content makes this assignment less likely. An alternative interpretation may be suggested from spectra recorded on mixed valence double sulfites. In spectra of such Chevreul's salts of copper, Cu^{+}-Cu^{2+} intervalence charge transfer bands are observed in the range 23 550–24 500 cm^{-1} (Inoue et al. 1999; da Silva et al. 2002). We suggest, in parallel with these examples, that a more likely origin of the broad band at ca. 24 000 cm^{-1} in our spectra of $Mg_{1-x}Cu_xAl_2O_4$ spinels is a Cu^{+}-Cu^{2+} intervalence electron transfer caused by a presence of trace amounts of monovalent copper that are charge compensated by subordinate excess amounts of Al^{3+}. Sufficient concentrations of Cu^{+}, and corresponding charge compensating Al^{3+}, to produce intervalence charge transfer bands of the intensities observed in the present spectra would be well below the detection limits of the presently applied electron microprobe and X-ray diffraction techniques. As the interatomic M-M distance is shorter than the corresponding T-M distance (in the present spinel series, about 2.86 and 3.35 Å, respectively) and as only M sites share edges in the spinel structure, we further suggest that this absorption band is caused by a $^{M}Cu^{+}$-$^{M}Cu^{2+}$ intervalence electron transfer process.

The observed splitting of the absorption band caused by electron transitions in $^{T}Cu^{2+}$ at ca. 7000 cm^{-1} into two components at ca. 6600 and 7400 cm^{-1} as well as the anomalous broadness of the absorption band caused by electron transitions in $^{M}Cu^{2+}$ at ca. 13 500 cm^{-1} indicates that divalent copper ions at both T and M sites are subject to local Jahn-Teller effects.

The almost constant weighted mean energy of the split absorption band due to spin-allowed transitions in $^{T}Cu^{2+}$ (bands ν_1 and ν_2 in Table 4) strongly suggest that the local $^{T}Cu^{2+}$-O bond length remains constant throughout the entire $Mg_{1-x}Cu_xAl_2O_4$ solid-solution series. This is an additional example of strong structural relaxation of TO_4 polyhedra in the spinel structure that suggests that they may virtually act as rigid building blocks throughout a spinel solid-solution series (Hålenius et al. 2011). In contrast, the slight energy decrease, at increasing Cu-content, from ca. 13 700 to 13 100 cm^{-1} for the absorption band due to the spin-allowed transition in $^{M}Cu^{2+}$ (band ν_3 in Table 4) suggests that local $^{M}Cu^{2+}$-O bond lengths are ca. 0.02 Å shorter in $MgAl_2O_4$ spinels containing trace amounts of copper as compared to $^{M}Cu^{2+}$-O bond lengths in end-member $CuAl_2O_4$ spinel.

Long-range structure

Although increasing Cu-contents along the $MgAl_2O_4$-$CuAl_2O_4$ series result in expected variations in the m.a.n. at the T and M sites (12.3–24.1 and 12.9–15.7, respectively) as a consequence of the higher atomic number of Cu ($Z = 29$) in relation to Mg and Al ($Z = 12$ and 13, respectively), very limited variations are observed in the unit-cell parameter *a* for this series: 8.079 to 8.087 Å ($\Delta a < 0.009$ Å). This is related to the strongly limited variations in the tetrahedral bond length from 1.913 to 1.920 Å rather than to the practically constant octahedral bond length 1.929–1.930 Å (Fig. 4). Although a limited decrease in *a*-parameter and T-O distance accompanies the increase in Cu-spinel component, the ultimate cause of the geometrical variations is mainly related to variations in Al content at the T site, i.e., to ordering effects. In fact, the substitution $Cu^{2+} \rightarrow Mg$ at the T site is expected to cause only minor T-O bond length changes because the two cations have quite similar radii: as mentioned before, the $^{T}Cu^{2+}$-O distance equals 1.960 Å, whereas $^{T}Mg^{2+}$-O is 1.966 Å. Consequently, the limited decrease in mean T-O

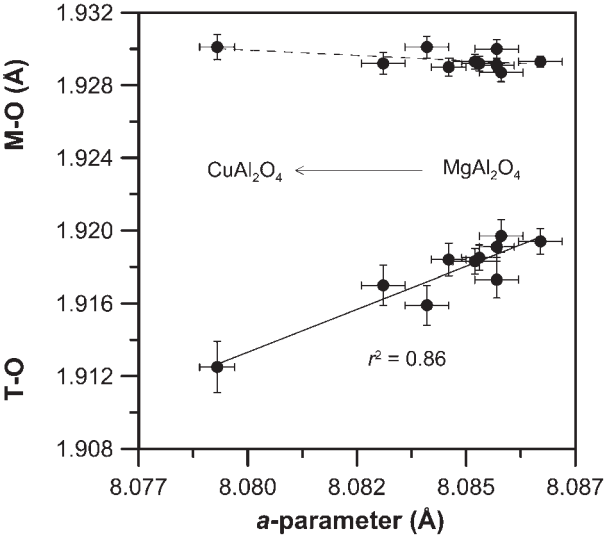

FIGURE 4. Variations in T-O and M-O bond lengths vs. the unit-cell parameter *a* in the $Mg_{1-x}Cu_xAl_2O_4$ spinel solid solution.

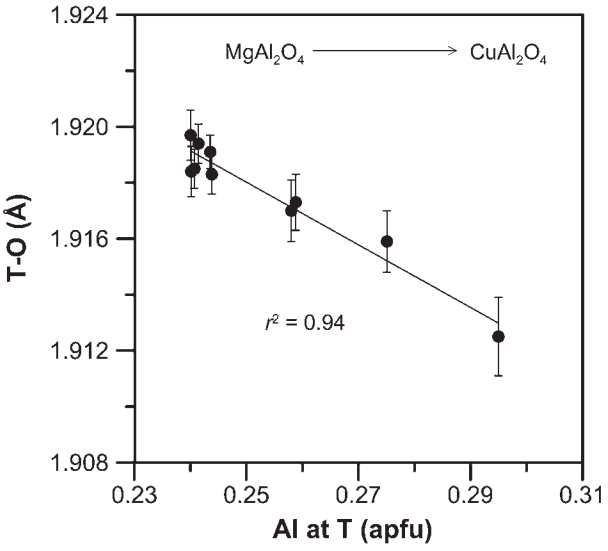

FIGURE 5. T-O distance vs. Al content at T sites in the $Mg_{1-x}Cu_xAl_2O_4$ spinel solid solution.

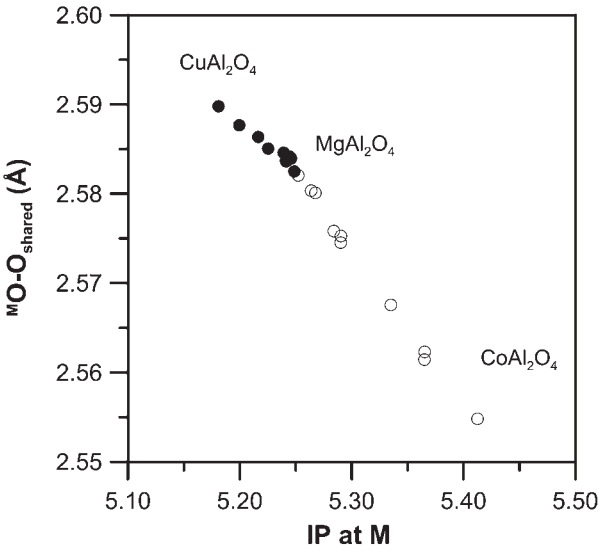

FIGURE 6. Variations in distances between shared oxygen atoms of MO_6 polyhedra vs. ionic potential of the cations at the M sites in the spinel solid-solution series $Mg_{1-x}Cu_xAl_2O_4$ (filled symbols = this work) and $Mg_{1-x}Co_xAl_2O_4$ (open symbols = Bosi et al. 2012, this issue).

distance from 1.920 to 1.913 Å with increasing incorporation of Cu in the structure can be mainly ascribed to an increase in Al content at the T site (Fig. 5).

The inversion degree and thus Al disordering over T and M sites slightly increases with the substitution $Cu^{2+} \rightarrow Mg$. The significant but small (0.24–0.29) variation in cation disordering is mainly related to the almost equal size of Mg and Cu^{2+} at the M site and concomitant non-equal sizes of Mg and Cu^{2+} at the T sites (steric effects). To illustrate how such steric effects drive the cation disordering, we have to consider that the substitution $Cu^{2+} \rightarrow Mg$ does not induce any variation in M-O but only a small decrease in T-O due to the increased ^{T}Al content. In accordance with Bosi et al. (2010), the increase in M-O/T-O ratio from 1.006 to 1.009 with increasing Cu^{2+} results in a reduction in the octahedral distortion as well as the oxygen fractional coordinate. As a result, the length of the shared octahedral edges, $^{M}(O\text{-}O)_{shared}$, increases from 2.584 to 2.590 Å, diminishing the oxygen shielding effect of the octahedral cation-cation repulsion (e.g., Lavina et al. 2003; Nakatsuka et al. 2003). The latter, in turn, decreases due to the lower $^{M}Al^{3+}$ and higher $^{M}Cu^{2+}$ contents. To describe the electrostatic cation-cation repulsion across $^{M}(O\text{-}O)_{shared}$ in the spinel structure in numerical terms, the ionic potential at M, ^{M}IP, may be useful (Bosi et al. 2011). ^{M}IP is calculated as the ratio of the aggregate formal valence of the cations occupying the M site to the aggregate cation radius at M obtained by the M-O distance minus 1.38 Å (i.e., the ionic radius of oxygen in fourfold coordination). Since ^{M}IP is proportional to the charge density at M, a decrease in ^{M}IP leads to an increase in $^{M}(O\text{-}O)_{shared}$, which provides a proportional oxygen shielding effect to the octahedral cation-cation repulsion. This effect was demonstrated for the $MgAl_2O_4$-$CoAl_2O_4$ series (Bosi et al. 2012, this issue), and a comparable correlation has been obtained for the present $Mg_{1-x}Cu_xAl_2O_4$ spinel series (Fig. 6).

In summary, due to the very similar sizes of Cu^{2+} and Mg at the T and M sites in the studied $MgAl_2O_4$-$CuAl_2O_4$ solid-solution series, the spinel structure responds to the $Cu^{2+} \rightarrow Mg$ substitution by increasing cation disorder in such a manner that the mean M-O distances remain constant, whereas the T-O distances decrease slightly. This results in increasing length of the $^{M}(O\text{-}O)_{shared}$, and thereby optimization of the octahedral cation-cation repulsion. In line with other studies, the importance of steric factors for controlling the cation distributions in the spinel structure has hence been shown to be valid also in the $MgAl_2O_4$-$CuAl_2O_4$ solid-solution series.

ACKNOWLEDGMENTS

Chemical analyses were carried out with the kind assistance of M. Serracino to whom the authors express their gratitude. Financial support from the SYNTHESYS program (grant SE-TAF-893, European Community, Research Infrastructure Action, FP7 CAPACITIES Programme) is gratefully acknowledged. The present work benefited from financial support of the Italian PRIN 2008 "SPIN GEO-TECH" and from the Swedish Research Council (VR). Constructive comments and suggestions by Richard Harrison and an anonymous reviewer improved the quality of this manuscript. We appreciate the careful manuscript handling by Simon Redfern.

REFERENCES CITED

Andreozzi, G.B. and Lucchesi, S. (2002) Intersite distribution of Fe^{2+} and Mg in the spinel (sensu stricto)–hercynite series by single crystal X-ray diffraction. American Mineralogist, 87, 1113–1120.

Bosi, F., Lucchesi, S., and Della Giusta, A. (2002) Structural relationships in $(Mn_{1-x}Zn_x)Mn_2O_4$ ($0 \le x \le 0.26$): the "dragging effect" of the tetrahedron on the octahedron. American Mineralogist, 87, 1121–1128.

Bosi, F., Andreozzi, G.B., Ferrini, V., and Lucchesi, S. (2004) Behavior of cation vacancy in kenotetrahedral Cr-spinels from Albanian eastern belt ophiolites. American Mineralogist, 89, 1367–1373.

Bosi, F., Hålenius, U., Andreozzi, G.B., Skogby, H., and Lucchesi, S. (2007) Structural refinement and crystal chemistry of Mn-doped spinel: A case for tetrahedrally coordinated Mn^{3+} in an oxygen-based structure. American Mineralogist, 92, 27–33.

Bosi, F., Hålenius, U., and Skogby, H. (2008) Stoichiometry of synthetic ulvöspinel single crystals. American Mineralogist, 93, 1312–1316.

——— (2009) Crystal chemistry of the magnetite-ulvöspinel series. American Mineralogist, 94, 181–189.

——— (2010) Crystal chemistry of the $MgAl_2O_4$-$MgMn_2O_4$-$MnMn_2O_4$ system: Analysis of structural distortion in spinel- and hausmannite-type structures. American Mineralogist, 95, 602–607.

Bosi, F., Andreozzi, G.B., Hålenius, U., and Skogby, H. (2011) Zn-O tetrahedral bond length variations in normal spinel oxides. American Mineralogist, 96, 594–598.

Bosi, F., Hålenius, U., D'Ippolito, V., and Andreozzi, G.B. (2012) Blue spinel crystals in the $MgAl_2O_4$-$CoAl_2O_4$ series: Part II. Cation ordering over short-range and long-range scales. American Mineralogist, 97, 1834–1840.

Burns, P.C. and Hawthorne, F.C. (1996) Static and dynamic Jahn-Teller effects in Cu^{2+} oxysalt minerals. Canadian Mineralogist, 34, 1089–l105.

Carbonin, S., Russo, U., and Della Giusta, A. (1996) Cation distribution in some natural spinels from X-ray diffraction and Mössbauer spectroscopy. Mineralogical Magazine, 60, 355–368.

da Silva, L.A., de Andrade, J.B., and Toma, H.E. (2002) Electronic spectra of Chevreul's salts. Journal of the Brazilian Chemical Society, 13, 624–628.

Dollase, W.A. and O'Neill, H.St.C. (1997) The spinels $CuCr_2O_4$ and $CuRh_2O_4$. Acta Crystallographica, C53, 657–659.

Fregola, R.A., Bosi, F., and Skogby, H. (2011) A first report on anion vacancies in a defect $MgAl_2O_4$ natural spinel. Periodico di Mineralogia, 80, 27–38.

Hålenius, U., Bosi, F., and Skogby, H. (2011) A first record of strong structural relaxation of TO_4 tetrahedra in a spinel solid solution. American Mineralogist, 96, 617–622.

Inoue, M., Grijalva, H., Inoue, M.B., and Fernando, Q. (1999) Spectroscopic and magnetic properties of Chevreul's salt, a mixed valence copper sulfite $Cu_3(SO_3)_2{\cdot}2H_2O$. Inorganica Chimica Acta, 295, 125–127.

Lavina, B., Salviulo, G., and Della Giusta, A. (2002) Cation distribution and structure modeling of spinel solid solutions. Physics and Chemistry of Minerals, 29, 10–18.

Lavina, B., Reznitskii, L.Z., and Bosi, F. (2003) Crystal chemistry of some Mg, Cr, V normal spinels from Sludyanka (Lake Baikal, Russia): the influence of V^{3+} on structural stability. Physics and Chemistry of Minerals, 30, 599–605.

Lenaz, D. and Princivalle, F. (2011) First occurrence of titanomagnetites from the websterite dykes within Balmuccia peridotite (Ivrea-Verbano zone): crystal chemistry and structural refinement. Periodico di Mineralogia, 80, 19–26.

Lenaz, D., Skogby, H., Princivalle, F., and Hålenius, U. (2004) Structural changes and valence states in the $MgCr_2O_4$-$FeCr_2O_4$ solid solution series. Physics and Chemistry of Minerals, 31, 633–642.

——— (2006) The $MgCr_2O_4$-$MgFe_2O_4$ solid solution series: effects of octahedrally coordinated Fe^{3+} on T-O bond lengths. Physics and Chemistry of Minerals, 33, 465–474.

Le Nestour, A., Gaudon, M., Villeneuve, G., Andriessen, R., and Demourgues, A. (2007a) Steric and electronic effects relating to the Cu^{2+} Jahn-Teller distortion in $Zn_{1-x}Cu_xAl_2O_4$ spinels. Inorganic Chemistry, 46, 2645–2658.

Le Nestour, A., Gaudon, M., Villeneuve, G., Daturi, M., Andriessen, R., and Demourgues, A. (2007b) Defects in divided zinc-copper aluminate spinels: structural features and optical absorption properties. Inorganic Chemistry, 46, 4067–4078.

Nakatsuka, A., Ikeda, Y., Yamasaki, Y., Nakayama, N., and Mizota, T. (2003) Cation distribution and bond lengths in $CoAl_2O_4$ spinel. Solid State Communications, 128, 85–90.

O'Neill, H.St.C., James, M., Dollase, W.A., and Redfern, S.A.T. (2005) Temperature dependence of the cation distribution in $CuAl_2O_4$ spinel. European Journal of Mineralogy, 17, 581–586.

Palin, E.J. and Harrison, R.J. (2007) A computational investigation of cation ordering phenomena in the binary spinel system $MgAl_2O_4$-$FeAl_2O_4$. Mineralogical Magazine, 71, 611–624.

Prince, E. and Treuting, R.G. (1956) The structure of tetragonal copper ferrite. Acta Crystallographica, 9, 1025–1028.

Pouchou, J.L. and Pichoir, F. (1984) A new model for quantitative X-ray microanalysis. I. Application to the analysis of homogeneous samples. La Recherche Aérospatiale, 3, 13–36.

Shannon, R.D. (1976) Revised effective ionic radii and systematic studies of interatomic distances in halides and chalcogenides. Acta Crystallographica, A32, 751–767.

Sheldrick, G.M. (2008) A short history of SHELX. Acta Crystallographica, A64, 112–122.

Tarantino, S.C., Zema, M., and Giannini, M. (2010) $Mg_xCu_{1-x}Cr_2O_4$ spinel solid solution: Jahn-Teller distortion and phase transitions. Acta Mineralogica-Petrographica Abstract Series, 6, IMA2010 Budapest, Hungary, 5.

MANUSCRIPT RECEIVED MARCH 26, 2012
MANUSCRIPT ACCEPTED JULY 16, 2012
MANUSCRIPT HANDLED BY SIMON REDFERN